

Multiaction Platinum(IV) Prodrug Containing Thymidylate Synthase Inhibitor and Metabolic Modifier against Triple-Negative Breast Cancer

Nafees Muhammad, Cai-Ping Tan,* Uroosa Nawaz, Jie Wang, Fang-Xin Wang, Sadia Nasreen, Liang-Nian Ji, and Zong-Wan Mao*



Cite This: <https://dx.doi.org/10.1021/acs.inorgchem.0c01736>



Read Online

ACCESS |



Metrics & More

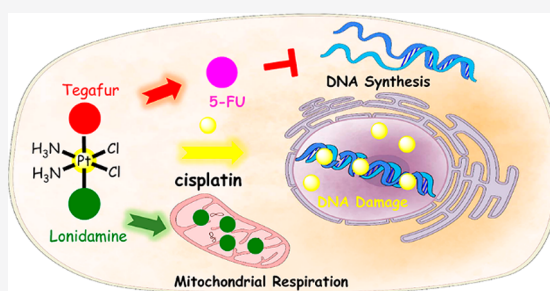


Article Recommendations



Supporting Information

ABSTRACT: Multifunctional platinum^{IV} anticancer prodrugs have the potential to enrich the anticancer properties and overcome the clinical problems of drug resistance and side effects of platinum^{II} anticancer agents. Herein, we develop dual and triple action platinum^{IV} complexes with targeted and biological active functionalities. One complex (PFL) that consists of cisplatin, tegafur, and lonidamine exhibits strong cytotoxicity against triple negative breast cancer (TNBC) cells. Cellular uptake and distribution studies reveal that PFL mainly accumulates in mitochondria. As a result, PFL disrupts the mitochondrial ultrastructure and induces significant alterations in the mitochondrial membrane potential, which further leads to an increase in production of reactive oxygen species (ROS) and a decrease in ATP synthesis in MDA-MB-231 TNBCs. Western blot analysis reveals the formation of ternary complex of thymidylate synthase, which shows the intracellular conversion of tegafur into 5-FU after its release from PFL. Furthermore, treatment with PFL impairs the mitochondrial function, leading to the inhibition of glycolysis and mitochondrial respiration and induction of apoptosis through the mitochondrial pathway. The RNA-sequencing experiment shows that PFL can perturb the pathways involved in DNA synthesis, DNA damage, metabolism, and transcriptional activity. These findings demonstrate that PFL intervenes in several cellular processes including DNA damage, thymidylate synthase inhibition, and perturbation of the mitochondrial bioenergetics to kill the cancer cells. The results highlight the significance of a triple-action prodrug for efficient anticancer therapy for TNBCs.



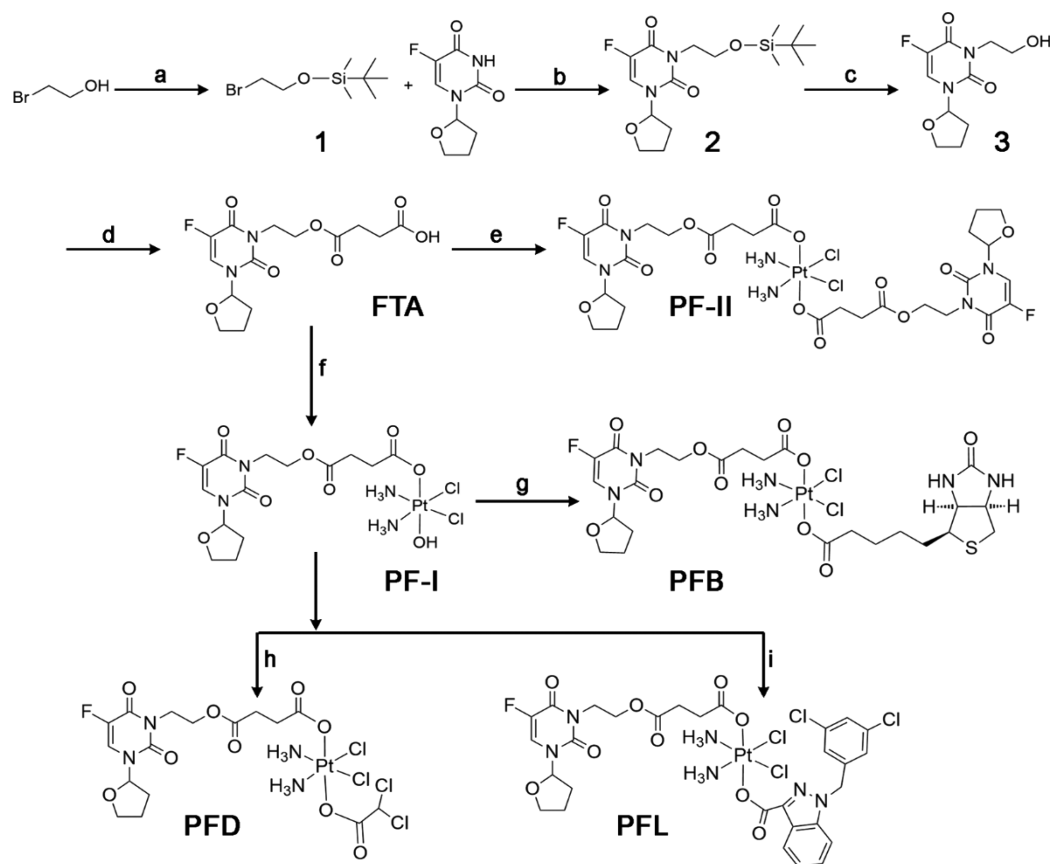
INTRODUCTION

Triple negative breast cancer (TNBC), characterized by lack of expression of estrogen, progesterone, and human epidermal growth factor receptor 2 (HER2), is the main cause of breast cancer mortality.¹ Conventional chemotherapy continues to play a pivotal role in the treatment of TNBC. However, clinical studies have proved that the efficacy of conventional drugs is limited by poor outcomes, drug resistance, and short duration response, which is caused by extensive intratumoral heterogeneity.² Cisplatin (cDDP) and its derivatives (carboplatin and oxaliplatin) are well-known for their high therapeutic efficacies against breast cancer.^{3,4} cDDP forms various forms of Pt-DNA cross-links that subsequently inhibits DNA metabolism and triggers cell death pathways.⁵ In spite of their success, clinically used platinum drugs may cause severe side effects and develop drug resistance.^{6–8}

Pt^{IV} complexes emerge as promising candidates to ameliorate the undesirable side effects of cDDP. The two additional axial positions on Pt^{IV} metal center offer extra opportunities to fine-tune the lipophilicity, bioavailability, and redox properties by selectively tethering biovectors or other biologically active molecules.^{9,10} Pt^{IV} complexes are generally regarded as prodrugs

as they are kinetically inert in the blood plasma compared with their parental compounds and can be activated upon reduction to Pt^{II} species. It is assumed that the higher concentration of biological reductants (e.g., glutathione and ascorbic acid (AA)) inside the cells helps to reduce the octahedral Pt^{IV} complexes to square planar cytotoxic Pt^{II} species. To date, Satraplatin is the only bioavailable Pt^{IV} based chemotherapeutic agent that was evaluated in a phase III clinical trial, but it failed to improve overall survival in a patient with hormone-refractory prostate tumor.¹¹ Recently, an increasing number of dual or triple action Pt^{IV} complexes have been developed, which opens up new possibilities to target different cellular targets with a single molecule.^{12–14}

Received: June 12, 2020

Scheme 1. Synthetic Routes of PF-I, PF-II, PFD, PFB, and PFL^a

^aConditions and reagents: (a) TBDMS, DCM, 12 h; (b) K_2CO_3 , ACN, reflux; (c) $Et_3N \cdot 3HF$, THF, 24 h; (d) succinic anhydride, ACN, 50 °C; (e) oxoplatin, TBTU, TEA, 48 h; (f) DMSO, RT, 72 h; (g) biotin, TBTU, TEA, 48 h; (h) DCA, 24 h; (i) lonidamine, TBTU, TEA, 48 h.

Tegafur (FT) is a prodrug of the antineoplastic agent 5-fluorouracil (5-FU) that shows mild toxicity and enhanced survival rates in patients with malignant tumors.¹⁵ The addition of a tetrahydrofuran (THF) moiety improves the antiangiogenic and cytotoxic performance of 5-FU.¹⁶ Upon cellular entrance, FT is converted to 5-FU (an inhibitor of thymidylate synthase (TS)) by the cytochrome P-450 enzyme.¹⁷ TS is crucial for the de novo synthesis of thymidylate (dTMP) that is required for the synthesis of DNA. TS is overexpressed in cancer cells (e.g., breast, prostate, kidney, and bladder), and elevated TS levels are thought to be associated with tumor invasiveness and metastasis.^{18–20} Biotin (vitamin B7) is an effective cancer-targeting moiety, as cancer cells proliferate actively and they require biotin as a growth promoter.²¹ Dichloroacetate (DCA) is an orphan drug that decreases the lactate level by inhibiting the pyruvate dehydrogenase kinase (PDK, an enzyme crucial for mitochondrial respiration).²² As demonstrated by Lippard et al., “mitaplatin” with two dichloroacetate moieties coordinated to the Pt^{IV} metal center at the axial positions can act as a dual-targeting molecule to overcome cDDP resistance.²³ Lonidamine (LN) is an indazole carboxylate that can selectively sensitize tumors when used in combination with other antineoplastic agents possibly by triggering the mitochondrial apoptotic pathway.^{24–26}

It remains unknown whether single-agent chemotherapy might be good for TNBC as chemo-resistance quickly develop after third to fourth cycle of treatment.²⁷ Therefore, the rationale behind the design of all complexes is to find a suitable candidate

which could induce multiple cellular events to execute cell death by overcoming the drug resistance associated with the use of single agent. In the present study, we report the synthesis and biological properties of Pt^{IV} prodrugs with FT coordinated at the axial positions (Scheme 1). To enhance the selectivity for cancer cells or achieve the combined effects on nuclei and mitochondria, biotin, DCA and lonidamine are used to construct the Pt^{IV} complexes with mixed axial ligands. We studied the selectivity of these complexes to TNBC cells. The anticancer mechanism of the most active agent, PFL, is investigated, which includes its intracellular reduction, cellular uptake and localization, effects on nuclear DNA damage and mitochondrial functions. Finally, the effect PFL on transcriptome is investigated by RNA sequencing. We demonstrate that PFL can effectively induce TNBC cell death by activating multicellular events.

RESULTS AND DISCUSSION

Synthesis and Characterization. The synthetic routes of PF-I, PF-II, PFD, PFB, and PFL are depicted in Scheme 1. Oxoplatin was synthesized in a manner reported previously.²⁸ The hydroxyl group of bromoethanol was first protected with tert-butyldimethylsilyl chloride (TBDMS) to yield intermediate 1 which then reacted with tegafur under refluxing acetonitrile (ACN) to give 2. Deprotection of silyl ether using $Et_3N \cdot 3HF$ give intermediate 3 which then reacted with succinic anhydride to give FTA. PF-II was synthesized by esterification reaction between FTA and oxoplatin in the presence of (1H-

Table 1. Cytotoxicity Profile of Pt^{IV} Compounds in Comparison to cDDP

	MDA-MB-231	MCF-7	A549	HepG2	MCF-10A
PF-I	6.1 ± 0.1	5.1 ± 0.2	9.2 ± 0.4	17.5 ± 1.2	8.1 ± 0.4
PF-II	29.4 ± 0.4	22.4 ± 0.5	27.5 ± 0.8	52.3 ± 1.1	22.2 ± 0.2
PFD	10.3 ± 0.4	8.2 ± 0.4	16.3 ± 0.5	13.2 ± 0.3	9.1 ± 0.3
PFB	21.5 ± 1.2	16.8 ± 0.5	32.2 ± 0.5	44.6 ± 1.2	28.8 ± 0.7
PFL	2.9 ± 0.2	4.8 ± 0.2	9.8 ± 0.4	10.7 ± 0.9	8.3 ± 0.1
cDDP	15.2 ± 0.1	4.1 ± 0.2	9.8 ± 0.2	13.5 ± 0.4	7.8 ± 0.3

benzotriazole-1-yl)-1,1,3,3-tetramethyluronium tetrafluoroborate (TBTU) and triethylamine (TEA). To obtain a high yield of PF-I, FTA-NHS ester (prepared by reacting FTA with 1-Ethyl-3-(3-dimethylaminopropyl)carbodiimide (EDC) and N-hydroxysuccinimide (NHS)) was used to react with oxoplatin in DMSO. PFB and PFL were then subsequently prepared by reaction of PF-I with biotin or lonidamine in the presence of TBTU and TEA. PFD was prepared by reacting PF-I with neat dichloroacetic anhydride (DCA). The complexes were characterized by (¹H, ¹³C and ¹⁹⁵Pt) NMR spectroscopy, ESI-MS spectrometry (Figure S1–S25, SI), and CHN elemental analysis. The ¹⁹⁵Pt NMR spectra show a single resonance peak at 1050, 1227, 1228, 1221, and 1225 ppm for PF-I, PF-II, PFD, PFB, and PFL, respectively. Prior to the biological evaluation, lipophilicity of Pt^{IV} complexes were measured because it might influence the antitumor properties of the Pt^{IV} prodrugs. All complexes were stable in phosphate buffer saline (PBS) over a period of 24 h as confirmed by high-performance liquid chromatography (HPLC; Figure S26). The lipophilicity (log *P*_{o/w}) of PF-I (−0.86), PF-II (−0.47), PFD (−0.52), PFB (−0.56), and PFL (−0.35) are measured using the shake flask method in a 1-octanol/phosphate buffer system (pH 7.4). The result indicates the monosubstituted complex (PF-I) is less lipophilic than the disubstituted complexes (PF-II, PFD, PFB, and PFL).

In Vitro Anticancer Activity. The cytotoxicity of the synthesized complexes was measured on a panel of human cancer cell lines including MDA-MB-231 (TNBC), MCF-7 (breast), A549 (lung), HepG2 (liver), and normal human mammary epithelial (MCF-10A) cells (Table 1). The half-maximal inhibitory concentrations (IC₅₀) of all the tested complexes are in the low micromolar range, whereas ligands FTA, DCA, and LN are found to be inactive (IC₅₀ > 60 μM). Among the synthesized complexes, PF-I and PFL are found to be more potent with IC₅₀ values comparable to those of cDDP against MCF-7 cells. Notably, PFL that consists of a TS inhibitor (FT) and the metabolic modifier (LN) shows about 5-fold higher cytotoxicity against MDA-MB-231 cells than cDDP. The cytotoxicities of the other dual-action complexes (PF-II, PFD, and PFB) are lower than that of cDDP in the cancer cell lines tested. PFB with a biotin moiety shows slightly higher cytotoxicity than PF-II. The low cellular uptake (vide infra) and slow reduction rate might be responsible for lower cytotoxicity of these disubstituted complexes.^{29,30} In addition, in MCF-10A cells, PF-I, PFD, and PFL display comparable cytotoxicity to cDDP, indicating that both complexes have increased cancer cell selectivity in the breast cancer cells.

Cellular Uptake. It has been reported that the intracellular accumulation of platinum drugs is associated with their cytotoxicity.³¹ So, we first determined the whole cell uptake of a synthesized complex in MDA-MB-231 carcinoma cells to interlink their cytotoxicity profile using inductively coupled plasma mass spectrometry (ICP-MS). As shown in Figure 1A,

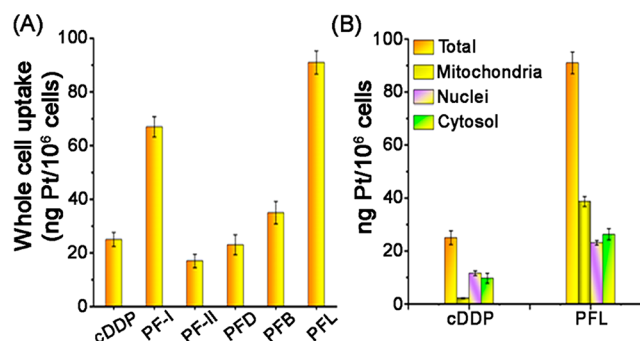


Figure 1. Content of Pt (ng/10⁶ cells) in MDA-MB-231 cells after treatment with 10 μM of PF-I, PF-II, PFD, PFB, or PFL for 24 h. (A) Whole cell uptake of platinum compounds. (B) Subcellular distribution of cDDP and PFL.

the uptake of PF-II is significantly (4-fold) lower than its monosubstituted complex (PF-I), which is in agreement with the related monosubstituted Pt^{IV} complexes.³² Unexpectedly, the addition of biotin moiety does not significantly increase the uptake of PFB compared with PFD, though both complexes share slightly similar lipophilicity. It is interesting to note that PFD shows a better cytotoxicity profile because of its multifunctional nature compared with PFB, though the uptake of the latter is higher than the former. This also indicates that uptake of Pt^{IV} complexes is only one of the parameters for better cytotoxicity. As PFL shows a broad spectrum of activity and is more potent against MDA-MB-231 cells than cDDP, it is chosen for further mechanistic investigations. The total platinum content associated with MDA-MB-231 cells upon treatment with PFL and cDDP is depicted in Figure 1B. cDDP treatment results in a much lower uptake in MDA-MB-231 cells than PFL (25 vs 91 ng Pt in 10⁶ cells). The subcellular distribution studies reveal that PFL mainly resides in mitochondria, while cDDP mainly accumulates in nuclei. The elevated Pt uptake and mitochondrial accumulation may contribute to the higher cytotoxicity of PFL.

Reduction Analysis with HPLC. As PF-I and PFL display the highest cellular uptake levels, we next examined their rate of reduction in the absence or presence of AA, a cellular reducing agent, over a period of 24 h using HPLC (Figures 2 and S27). Both complexes are stable in the absence of AA, whereas in the presence of AA, the absorption peak of PF-I decreases rapidly and the peak of FTA increases simultaneously. In contrast, PFL is reduced less quickly than PF-I under the same conditions. After 6 h, the percentage of PFL remained drops to about 9%, and the value increases to 39% after 12 h. It was suggested that the rate of reduction depends upon the electron transfer from the reductant to the Pt^{IV} metal center that results in the formation of a bridge between the Pt^{IV} complex and the reducing agent. Hydroxyl ligands in the coordination sphere would greatly facilitate the electron transfer process compared with

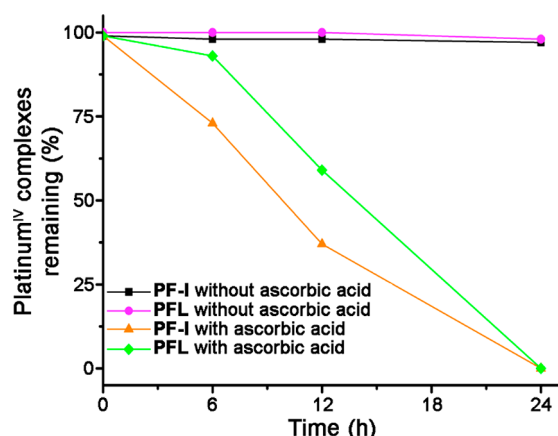


Figure 2. RP-HPLC analysis of remaining platinum^{IV} complexes. 500 μM of Pt^{IV} complexes were incubated with and without the presence of 5 mM AA in a solution of PBS/MeOH (9/1, V/V, pH 7.4) at 37 °C in the dark.

carboxylate;²⁹ therefore, we observed the faster reduction rate of PF-I compared with PFL. Both complexes are completely reduced after incubation with AA for 24 h.

Mechanism of Cytotoxicity. It is well-known that platinum-based anticancer drugs target nuclear DNA (ncDNA) in initiating their anticancer effect in tumor cells.³³ Therefore, we first use confocal microscopy to study the possible DNA damage upon treatment with PFL. As shown in Figure S28A, treatment of MDA-MB-231 cells with higher concentrations of PFL induces severe DNA fragmentation compared with cDDP, which confirms its ability to cause cellular DNA damage. We also studied the Pt levels on the genomic DNA of MDA-MB-231 cells (Figure S28B, SI). MDA-MB-231 cells treated with cDDP (10 μM) and PFL (10 μM) show 9.7 and 2.4 ng Pt per μg of DNA, respectively. These results are inconsistent

with the respective accumulation of PFL in nuclei, indicating that damaging nDNA may also play a critical role in anticancer mechanism of PFL.

We next examined apoptosis induced by PFL using annexin-V/propidium iodide (PI) double staining that can differentiate intact cells (annexin V-/PI-), early apoptotic (annexin V+/PI-), late apoptotic (annexin V+/PI+), and necrotic (Annexin V-/PI+) cells (Figure 3A). After treatment with PFL (10 μM), the percentage of early apoptotic cells (52.7%) significantly increases compared with control (5.58%), which is higher than cDDP (12.8%). The higher potency of PFL to induce apoptosis is in line with the cytotoxicity data. Next, the impact of PFL on cell cycle distribution is examined by flow cytometry (Figure 3B). PFL arrests the cell cycle in S phase, which is similar to that of cDDP, but its potency was much stronger than cDDP.³⁴ In untreated samples, the fraction of S-phase cells is 23%, and the fraction increases up to 60% with a concomitant decrease in G2 phase and an increase in G0/G1 phase when the cells were treated with 10 μM of PFL.

Mitochondria play vital and lethal functions in both physiological and pathological scenarios, as they are key regulators of energy production and crucial regulators for apoptotic machinery.³⁵ Since the alteration in the mitochondrial morphology is mechanistically interlinked with its functions, we hence examined the mitochondrial ultrastructure of MDA-MB-231 cells using transmission electron microscopy (TEM). Mitochondria in untreated cells show integral double membrane structure and physical coordination of polymorphic cristae exist within the mitochondrial matrix (Figure 4). In contrast, the portion of intact mitochondria decreases significantly in PFL-treated cells. Furthermore, PFL treatment induces mitochondrial swelling (a common feature of membrane permeabilization) and disrupts cristae (Figure 5 inset, indicated with white arrows). In addition, some autophagosomes which are generated as a result of autophagy and multivesicular bodies are also observed in MDA-MB-231 cells treated with PFL (Figure 4

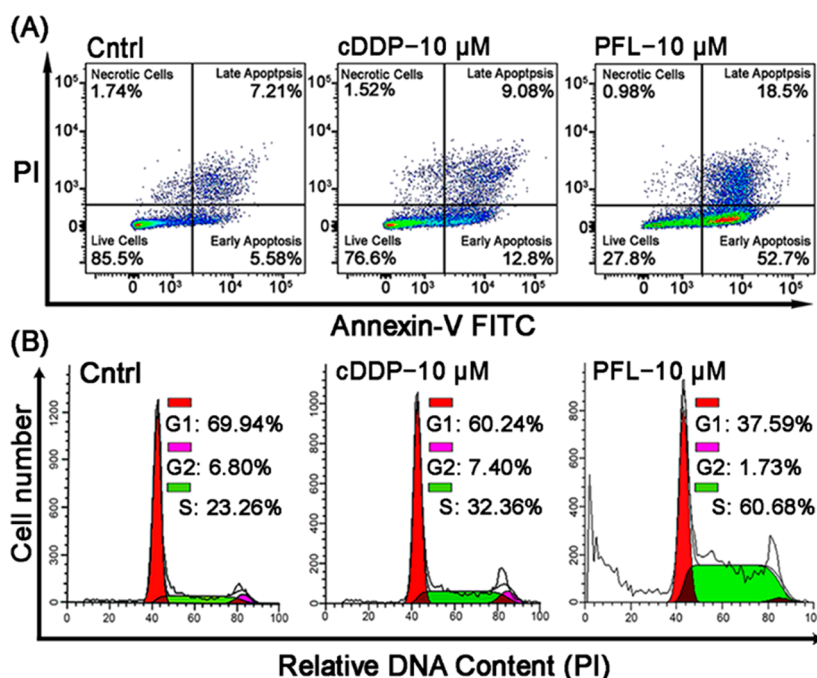


Figure 3. Impact of PFL on apoptosis and cell cycle analysis. (A) Flow cytometry analysis of MDA-MB-231 cells treated with cDDP and PFL for 48 h, followed by staining with annexin-V FITC and PI. (B) Cell cycle arrest of MDA-MB-231 cells treated with cDDP and PFL for 48 h.

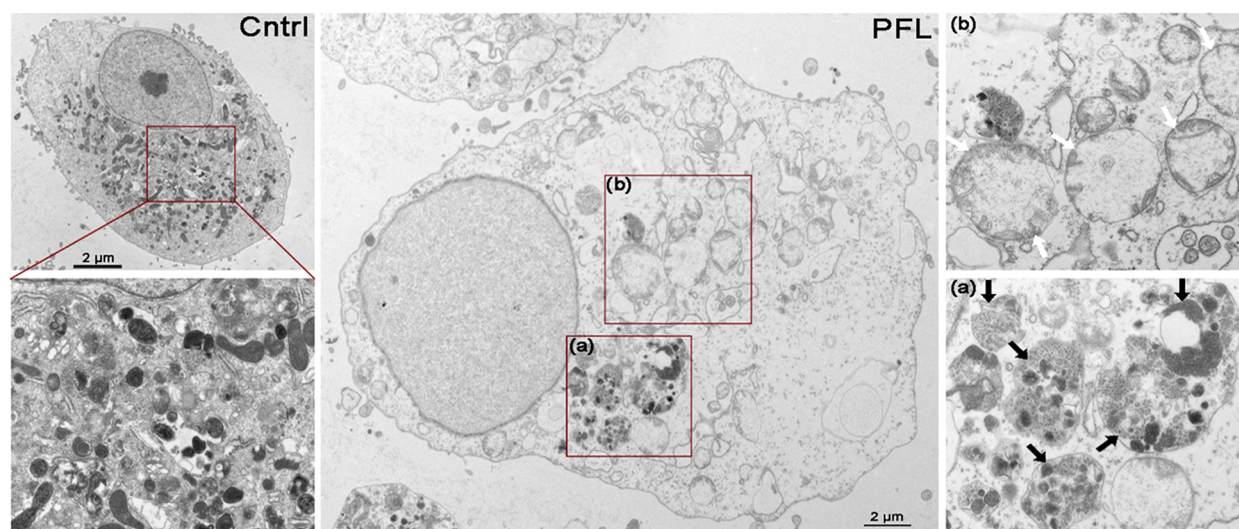


Figure 4. TEM images of mitochondria structure in MDA-MB-231 cells treated with or without PFL ($10 \mu\text{M}$) for 30 h.

inset, indicated with black arrows). As demonstrated above, PFL specifically accumulates in mitochondria and induces mitochondrial swelling in cells; therefore, its impact on mitochondrial membrane potential (MMP) is examined using 5,5',6,6'-tetrachloro-1,1',3,3'-tetraethyl-imidacarbocyanine iodide (JC-1) staining and flow cytometry. As shown in Figure 5A, the MMP in control cells is high where JC-1 assembles to form J aggregates (red fluorescence). After treatment with PFL, a marked decrease in MMP is observed as the JC-1 fluorescence shifts from red to green. The percentages of cells with depolarized mitochondria increase from $3.5 \pm 1.5\%$ (Control) to $67.3 \pm 5.7\%$ (PFL, $15 \mu\text{M}$). These findings are consistent with our WB results (vide infra), where the release of cytochrome C linked to loss of MMP. Mitochondria are indispensable for energy production and hence the survival of cells; therefore, as a consequence of loss of MMP, cellular ATP production should be perturbed. To confirm this, the impact of PFL on intracellular ATP production in MDA-MB-231 cells is measured with an ATP assay kit. Treatment with PFL results in a significant dose-dependent decrease in ATP production as compared with the control cells (Figure S29). These findings are similar to previous reports where lonidamine alone triggers ATP depletion in breast xenograft models.³⁶

Destruction of mitochondrial dynamics function could also influence the intracellular redox homeostasis; thus, intracellular ROS level was tracked by flow cytometry using 2',7'-dichlorofluorescein diacetate ($\text{H}_2\text{DCF-DA}$) ROS probe. As shown in Figure 5B, a dose-dependent increase of ROS production was observed in MDA-MB-231 cells after treatment with PFL for 30 h. Compared with the control cells, a 4-fold increase in ROS production was observed in cells treated with PFL at a dose of $10 \mu\text{M}$.

Next, we measured the oxygen consumption rate (OCR) in MDA-MB-231 cells upon treatment with PFL using a Seahorse XF24 extracellular flux analyzer. As shown in Figure 5C, exposure to PFL results in a significant impact on mitochondrial respiration. The data show that basal respiration dramatically decreases upon treatment with PFL compared with the control in a dose-dependent manner. Addition of oligomycin followed by mitochondrial uncoupler carbonyl cyanide 4-(trifluoromethoxy)phenylhydrazone (FCCP) into the media markedly reduces ATP synthase, maximal mitochondrial

respiration and spare capacity (Figure 5D). These results suggest that PFL has a strong impact on mitochondrial bioenergetics of MDA-MB-231 cells.

As lonidamine can inhibit glycolysis in cancer cells, we then determined the effect of PFL on aerobic glycolysis of MDA-MB-231 cells by measuring the extracellular acidification rate (ECAR). As shown in Figure 5E, ECAR is decreased in a dose-dependent manner upon PFL treatment. Changes in ECAR in response to sequential addition of glycolysis modulators (glucose, oligomycin, and 2-deoxy-D-glucose (2-DG)) to MDA-MB-231 cells were defined to determine the indices of glycolysis, glycolytic capacity, and glycolytic reserves. As expected, all these indices measured for PFL-treated cells (Figure 5F) were substantially lower than those for the control samples under the same conditions.

To further shed light on the mechanisms involved in the PFL-induced apoptosis, we investigated the impact of PFL on the expression of Bcl-2 family proteins including antiapoptotic (Bcl-2) and proapoptotic (Bax) proteins that play important roles in the mitochondrial pathway of apoptosis. The integrity of outer mitochondrial membrane (OMM) is control by Bcl-2 family of proteins that oligomerize into proteolipid pores and permeabilize the OMM, allowing the efflux of cytochrome c and other intermembrane space proteins to the cytosol during apoptosis.³⁷ Western blot data was used to study the expressions of Bcl-2, Bax, and Cyto c in MDA-MB-231 cells after treatment with PFL. As expected, the expression of Cytochrome C and Bax is significantly upregulated, while BCL-2 expression is down-regulated upon treatment with PFL (Figure 6A). These results indicate that PFL can activate apoptosis mediated by mitochondrial pathway. In addition, we investigated the TS expression using TS 106 monoclonal antibody (Figure 6B). PFL treatment significantly upregulates TS expression by forming a ternary complex (38 kDa) which confirms that FT is converted to 5-FU in the MDA-MB-231 cells and subsequently inhibits the TS enzyme.

RNA-seq Analysis. The impact of PFL on transcriptome was further investigated by comparing the gene expression profiles in TNBC cells. A correlation coefficient above 0.9 was observed between cells from the same group containing 3 individual samples (Figure S30). More than 97% of readings are mapped to reference genes in all samples, and 83% of readings

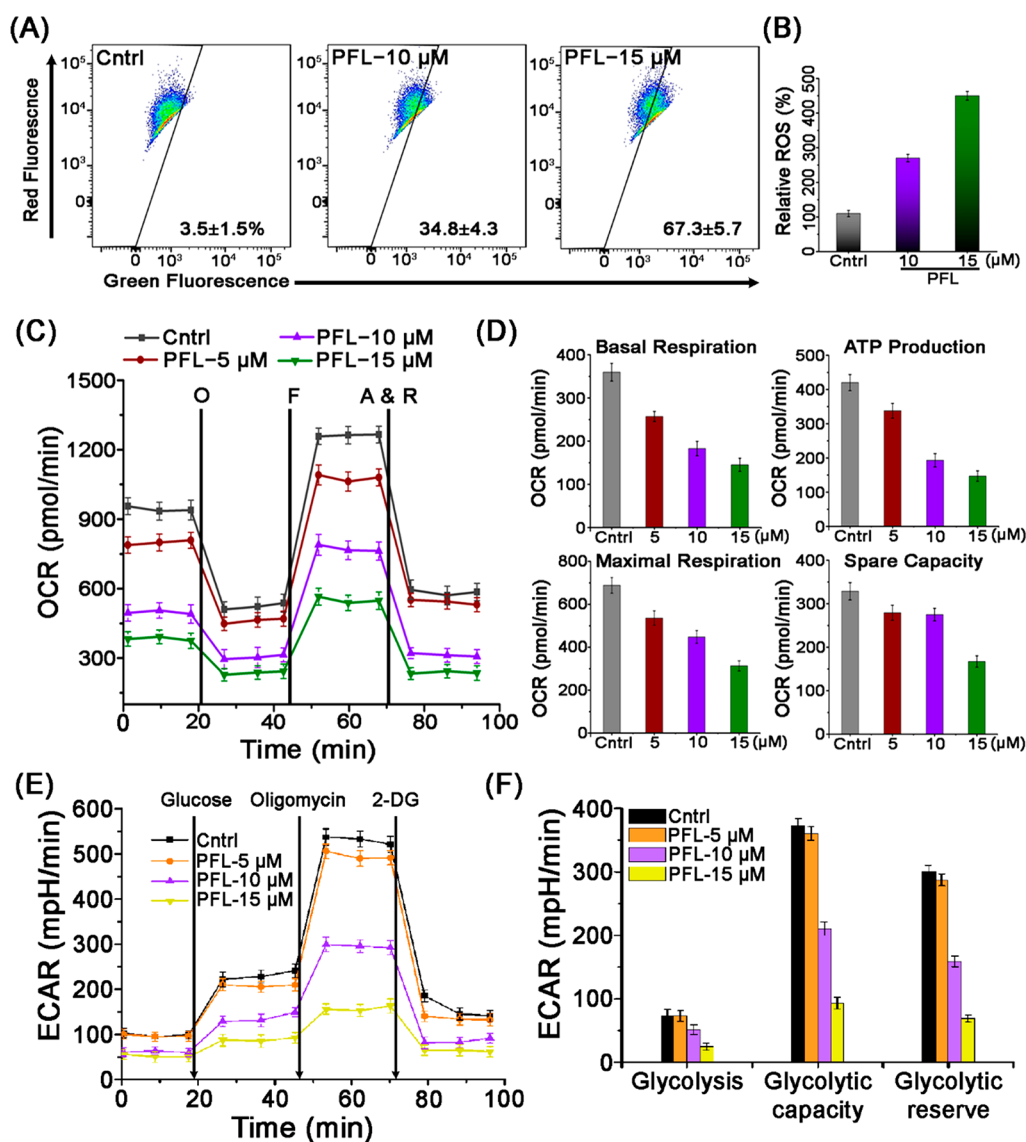


Figure 5. Detection of MMP by JC-1 staining after treatment with varying concentration of PFL. (A) Generation of ROS in MDA-MB-231 cells after incubation with PFL for 30 h. (B) Respiratory profile of PFL treated MDA-MB-231 cells after the addition of oligomycin (O), FCCP (F), and the mixture of antimycin and rotenone (A&R). The data are presented as the mean \pm SD ($n = 3$). (C) Key parameters of mitochondrial respiration. (D) Glycolysis profile of MDA-MB-231 cells after treatment with PFL for 30 h by a Seahorse XF24 Extracellular Flux Analyzer (E and F).

were located in exons (Figure S31). Among the 2992 genes that are significantly changed in the expression levels, 996 genes are upregulated and 1996 genes are downregulated (Figure 7A and Table S1). The heatmap of RNA-Seq shows that expression patterns are very similar classes are assigned to cluster different genes with putative functions (Figure S32). PFL treatment causes significant overall changes in gene categories including cellular process, biological regulation, cell part, organelle, binding, and catalytic activity (Figure S33). The genes are further analyzed by KEGG (Kyoto Encyclopedia of Genes and Genomes) pathway annotation. Various pathways for cancer progression such as PI3K-Akt signaling pathway and MPK signaling pathway are regulated by PFL treatment (Figure S34). Gene Set Enrichment Analysis (GSEA) reveals that gene expression profile of TNBC cells treated with PFL is negatively associated with DNA synthesis, DNA damage, metabolism, and positively related to transcriptional regulator activity (Figure 7). Interestingly, of all the 2992 genes with significant changes after PFL treatment, 1414 genes were related to transcription factor

(TF). Among them, 499 TF genes were up-regulated and 965 TF genes were down-regulated (Figure S34 and Table S2). Most of these genes belong to the high mobility group (HMG, 576 genes) and zinc finger C2H2 (ZF-C2H2, 403 genes) family (Figure 7C). The results are consistent with previous findings, indicating that cDDP can influence the activity of transcription factors, especially for HMG transcription factors.^{38–41}

CONCLUSIONS

Platinum^{IV} complexes emerge as promising candidates in recent years to ameliorate the undesirable side effects of cDDP and its analogues. These complexes act as a prodrug in blood plasma and can only be activated once inside the cell with the biological reductant that are abundantly expressed in cancer cells. In this study, we developed a series of both dual and triple action Pt^{IV} complexes and studied their in vitro anticancer activity against a panel of human cancer cell lines. The antiproliferative potency of these complexes are correlated with their cellular uptake efficacy. One of the most active complex, PFL, which consists of a

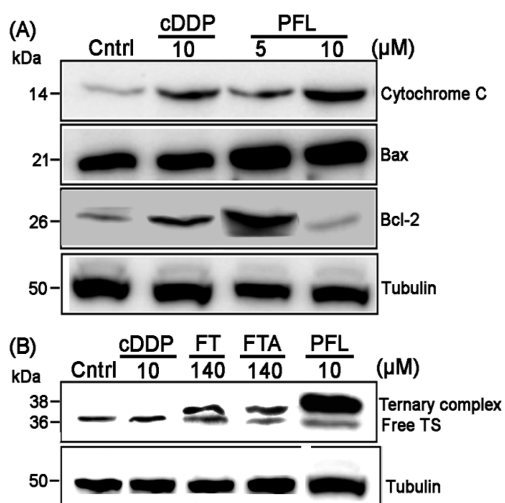


Figure 6. Expression of BCL-2, Bax, and Cyto C in MDA-MB-231 cells after treatment with cDDP or PFL (A). Expression of TS in MDA-MB-231 cells after treatment with cDDP, FT, FTA, and PFL for 48 h (B).

thymidylate synthase inhibitor and a metabolic modifier, exhibits enhanced anticancer activity against TNBC cells.

Subsequent investigations reveal that the PFL induces cell cycle arrest in S phase. Cellular distribution studies reveal that PFL mainly accumulates in mitochondria; hence, we carry out in depth mechanistic investigation to study the molecular mechanism involved in PFL-induced apoptosis. To do so, first we employed TEM to study the effect of PFL treatment onto mitochondrial inner membrane topology of MDA-MB-231 carcinoma cells. PFL exposure induces sewer mitochondrial swelling and disrupts cristae which are interlinked with a marked decrease in MMP as observed with JC-1 fluorescence shifts from red to green. Furthermore, treatment with PFL reduces cellular ATP production, inhibits the mitochondrial respiration, and elevates the level of ROS production. Western blot analysis reveals that PFL treatment significantly changes expression level of Bcl-2 family of proteins (Bcl-2, Bax), which eventually leads to the release of cytochrome C from mitochondria. In addition, Western blot analysis shows the formation of ternary complex of thymidylate synthase, which confirms the release of tegafur from the coordination sphere of PFL and its subsequent conversion to 5-FU inside the cells. RNA seq transcriptome analysis reveals that PFL can perturb the pathways involved in DNA synthesis, DNA damage, metabolism and those positively related to transcriptional regulator activity. These results provide new

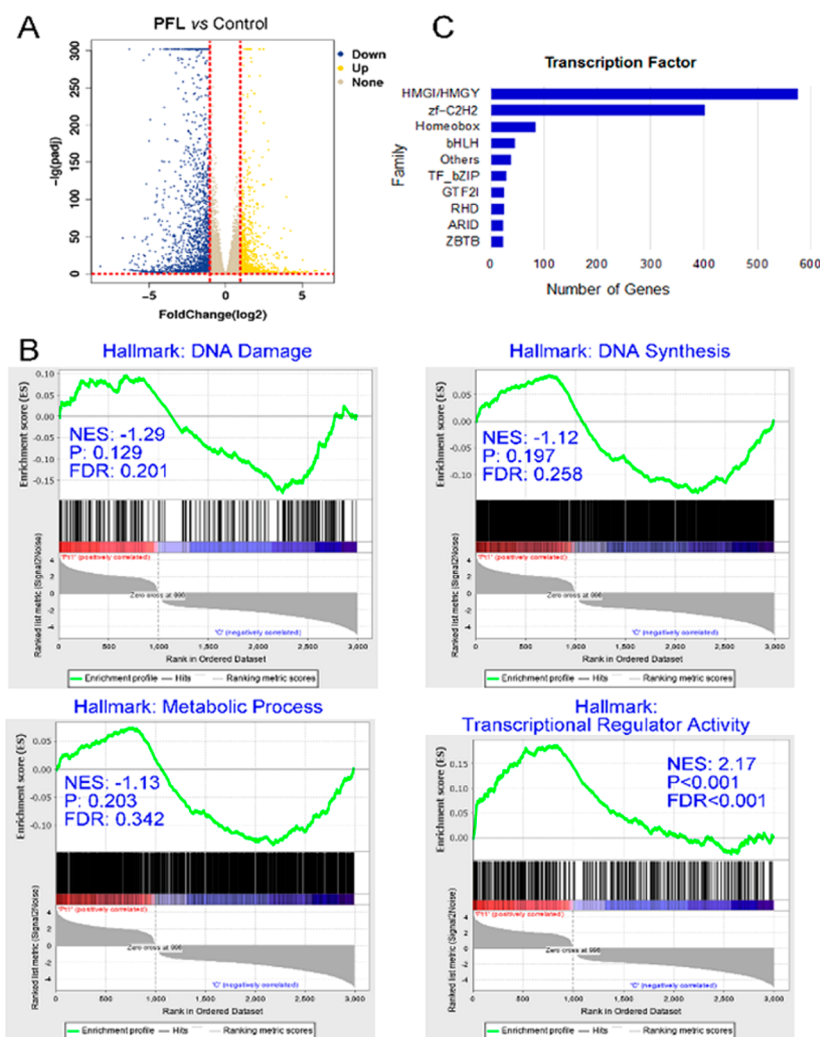


Figure 7. (A) Volcano plots showing the differentially expressed genes in MDA-MB-231 cells treated with PFL (10 μ M). (B) GSEA of PFL-altered genes in various cellular processes. (C) The top 10 transcription factor families with the largest number of significantly different genes.

insight into the development of multiaction Pt^{IV} complexes that activate multiple cellular events for the treatment of TNBC.

EXPERIMENTAL SECTION

Synthesis of 1. 2-Bromoethanol (6 g, 48 mmol) was added to a mixture of imidazole (3.6 g, 52 mmol) and *tert*-butyldimethylsilyl chloride (7.6 g, 50 mmol) in anhydrous DCM (40 mL). The reaction mixture was stirred at 0 °C for 30 min followed by stirring at RT for 12 h. After completion, the solvent was removed by a rotary evaporator, and the oily liquid was redissolved in ethyl acetate and then washed with water (20 mL × 2) and saturated NaCl (20 mL × 2). The solution was dried over Na₂SO₄. Evaporation of solvent yielded a colorless liquid (yield 90%). ¹H NMR (DMSO-*d*₆) δ (ppm) 0.11 (s, 6H), 0.93 (s, 9H), 3.40–3.43 (m, 2H), 3.90–3.93 (m, 2H).

Synthesis of 2. (2-Bromoethoxy)-*tert*-butyldimethylsilane 1 (6 g, 25 mmol) was added to a stirred suspension of tegafur (1 g, 5 mmol), K₂CO₃ (3.4 g, 25 mmol), and KI (0.5 mmol) in dry acetonitrile (150 mL). The reaction mixture was heated to reflux for 36 h, cooled to room temperature, and filtered. The filtrate was concentrated in vacuo, and the residue was purified by column chromatography using dichloromethane (100%) to yield 2 as a viscous oil (72%). ¹H NMR (DMSO-*d*₆) δ (ppm) 0.03 (s, 6H), 0.81 (s, 9H), 1.84–2.04 (m, 3H), 2.21–2.30 (m, 1H), 3.71–3.75 (t, 2H), 3.79–3.85 (q, 1H), 3.93–3.96 (t, 2H), 4.24–4.29 (m, 1H), 5.93–5.96 (m, 1H), 7.94–7.95 (d, 1H).

Synthesis of 3. In a 50 mL single-neck flask equipped with magnetic stirrer, 2 (1.70 g, 4.74 mmol) was dissolved in dry THF (20 mL) under a nitrogen atmosphere. Et₃N·3HF (1.69 g, 6.6 mmol) was then added dropwise, and the reaction mixture was stirred at room temperature. TLC shows the completion of the reaction after 24 h. Solvent was then evaporated, and the residue was purified by column chromatography using CH₂Cl₂/MeOH (95:5). ¹H NMR (DMSO-*d*₆) δ (ppm) 1.89–2.06 (m, 3H), 2.21–2.30 (m, 1H), 3.50–3.54 (q, 2H), 3.79–3.85 (q, 1H), 3.88–3.93 (m, 2H), 4.24–4.29 (m, 1H), 4.76–4.79 (t, 1H), 5.95–5.98 (m, 1H), 7.91–7.93 (d, 1H).

Synthesis of FTA. To a solution of 3 (1.05 g, 4.30 mmol) in dry acetonitrile was added TEA (630 μL) and succinic anhydride (520 mg, 5.17 mmol), and the reaction mixture was stirred at 50 °C overnight. Upon completion of the reaction, the solvent was rotary evaporated, and the residue was purified by column chromatography using CH₂Cl₂/MeOH (85:15). ¹H NMR (DMSO-*d*₆) δ (ppm) 1.91–2.07 (m, 3H), 2.21–2.30 (m, 1H), 2.42–2.44 (d, 4H), 3.80–3.86 (q, 1H), 4.04–4.07 (t, 2H), 4.20–4.30 (m, 3H), 5.93–5.96 (m, 1H), 7.93–7.95 (d, 1H), 12.22 (s, 1H).

Synthesis of PF-I. To a stirred suspension of oxoplatin (200 mg, 0.59 mmol) in dry DMSO was added FTA-NHS ester (265 mg, 0.60 mmol) previously prepared by reacting FTA with EDC and NHS. The reaction mixture was stirred at room temperature for 3 days. A clear yellow solution was obtained upon completion of reaction. Solvent was reduced to half, and the product was extracted by repetitive washing with diethyl ether. ¹H NMR (DMSO-*d*₆) δ (ppm) 1.89–2.08 (m, 3H), 2.23–2.30 (m, 1H), 2.38–2.41 (m, 3H), 3.80–3.86 (q, 1H), 4.05–4.07 (t, 2H), 4.20–4.30 (m, 3H), 5.79–6.05 (m, 7H), 7.94–7.96 (d, 1H). ¹³C NMR (DMSO-*d*₆) δ (ppm) 23.95, 30.52, 31.49, 32.19, 60.91, 70.10, 87.94, 124.15, 138.65, 140.91, 149.29, 156.98, 157.23, 172.92, 179.69. ¹⁹⁵Pt NMR (DMSO-*d*₆): 1050 ppm. ESI-MS (negative mode, *m/z*): 660.12, elemental analysis calculated (%) for Pt-(NH₃)₂Cl₂(C₁₄H₁₆FN₂O₇)OH (Mw = 660.35): C 25.46, H 3.51, N 8.48; found: C 25.20, H 3.48, N 8.53.

Synthesis of PF-II. To a stirred suspension of oxoplatin (100 mg, 0.29 mmol) in dry DMF was added 4 (220 mg, 0.64 mmol), TBTU (205 mg, 0.64 mmol) and TEA (82 μL). The reaction mixture was stirred at room temperature for 48 h. A clear yellow solution was obtained upon completion of reaction. Solvent was evaporated in vacuo, and the product was purified by column chromatography using CH₂Cl₂/MeOH (70:30). ¹H NMR (DMSO-*d*₆) δ (ppm) 1.88–2.08 (m, 8H), 2.21–2.30 (m, 2H), 2.31–2.46 (m, 6H), 3.79–3.84 (q, 2H), 4.03–4.06 (t, 4H), 4.20–4.28 (m, 6H), 5.92–5.95 (m, 2H), 6.34–6.57 (m, 6H), 7.93–7.95 (d, 2H). ¹³C NMR (DMSO-*d*₆) δ (ppm) 23.95, 30.18, 30.68, 32.19, 61.02, 70.10, 87.94, 124.15, 124.49, 138.65, 140.92,

149.29, 156.99, 157.25, 172.64, 179.56. ¹⁹⁵Pt NMR (DMSO-*d*₆): 1227 ppm. ESI-MS (negative mode, *m/z*): 985.46 (M-H), elemental analysis calculated (%) for Pt(NH₃)₂Cl₂(C₂₈H₃₂F₂N₄O₁₄) (Mw = 986.63): C 34.08, H 3.88, N 8.52; found: C 34.15, H 3.76, N 8.45.

Synthesis of PFD. To a stirred suspension of PF-I (130 mg, 0.19 mmol) in dry DCM was added DCA anhydride (140 μL, 1 mmol). The reaction mixture was stirred at room temperature for 24 h. After completion of reaction, addition of diethyl ether quickly precipitated the desired product which was washed several times with diethyl ether and dried in vacuo. Yield 70%. ¹H NMR (DMSO-*d*₆) δ (ppm) 1.91–2.05 (m, 3H), 2.23–2.32 (m, 1H), 2.38–2.41 (m, 2H), 3.80–3.86 (q, 1H), 4.06–4.08 (d, 2H), 4.22–4.29 (m, 3H), 5.95 (s, 1H), 6.22–6.83 (m, 7H), 7.94–7.96 (d, 1H). ¹³C NMR (DMSO-*d*₆) δ (ppm) 23.96, 30.15, 30.42, 32.18, 61.05, 66.20, 70.10, 87.94, 124.17, 124.50, 138.65, 140.92, 149.30, 157.00, 157.25, 170.95, 172.50, 179.51. ¹⁹⁵Pt NMR (DMSO-*d*₆): 1221 ppm. ESI-MS (negative mode, *m/z*): 769.77, elemental analysis calculated (%) for [Pt-(NH₃)₂Cl₂(C₁₆H₁₇C₁₂FN₂O₉)] (Mw = 770.29): C 24.92, H 3.01, N 7.26; found: C 24.82, H 3.11, N 7.23.

Synthesis of PFB. To a stirred suspension of PF-I (100 mg, 0.15 mmol) in dry DMSO was added biotin (40 mg, 0.16 mmol), TBTU (51 mg, 0.16 mmol), and TEA (21 μL). The reaction mixture was stirred at room temperature for 48 h. TLC shows the completion of reaction. Solvent was evaporated in vacuo, and the product was purified by column chromatography using CH₂Cl₂/MeOH (40:60). ¹H NMR (DMSO-*d*₆) δ (ppm) 1.27–1.67 (m, 7H), 1.92–2.05 (m-3H), 1.92–2.05 (m, 3H), 2.21–2.30 (m, 3H), 2.37–2.41 (t, 2H), 2.57–2.60 (d, 1H), 2.81–2.85 (dd, 1H), 3.08–3.13 (dd, 1H), 3.80–3.86 (q, 1H), 4.07–4.08 (d, 2H), 4.14–4.33 (m, 5H), 5.95 (s, 1H), 6.36–6.68 (m, 8H), 7.94–7.96 (d, 1H). ¹³C NMR (DMSO-*d*₆) δ (ppm) 23.96, 25.92, 28.55, 30.21, 30.74, 32.18, 35.97, 55.89, 59.68, 61.02, 61.50, 70.10, 87.94, 124.16, 124.50, 138.65, 140.91, 149.30, 156.99, 157.25, 162.80, 163.21, 172.66, 179.57, 181.27. ¹⁹⁵Pt NMR (DMSO-*d*₆): 1229 ppm. ESI-MS (negative mode, *m/z*): 885.29, elemental analysis calculated (%) for [Pt(NH₃)₂C₁₂(C₂₄H₃₁FN₄O₁₀S)] (Mw = 886.64): C 32.51, H 4.21, N 9.48; found: C 32.31, H 4.26, N 9.45.

Synthesis of PFL. To a stirred suspension of PF-I (130 mg, 0.19 mmol) in dry DMF was added lonidamine (81 mg, 0.25 mmol), TBTU (82 mg, 0.25 mmol), and TEA (38 μL, 0.25 mmol). The reaction mixture was stirred at room temperature for 48 h. Upon completion of reaction, the solvent was evaporated, and the residue was purified using CH₂Cl₂/MeOH (95:5). ¹H NMR (DMSO-*d*₆) δ (ppm) 1.87–2.08 (m, 3H), 2.23–2.33 (m-1H), 2.41–2.44 (t, 2H), 3.81–3.86 (q, 1H), 4.03–4.09 (m, 2H), 4.24–4.30 (m, 2H), 5.78–5.83 (t, 2H), 5.96 (s, 1H), 6.38–6.99 (m, 7H), 7.27–7.32 (t, 1H), 7.37–7.46 (m, 4H), 7.69–7.79 (m, 2H), 7.95–7.96 (d, 1H), 8.32–8.34 (d, 1H). ¹³C NMR (DMSO-*d*₆) δ (ppm) 23.96, 30.22, 30.69, 32.19, 49.97, 61.05, 70.14, 87.96, 110.41, 122.69, 123.57, 124.05, 124.18, 127.23, 128.13, 129.51, 131.14, 133.61, 134.0, 141.12, 149.25, 157.16, 172.64, 179.63. ¹⁹⁵Pt NMR (DMSO-*d*₆): 1225 ppm. ESI-MS (negative mode, *m/z*): 961.23, elemental analysis calculated (%) for [Pt-(NH₃)₂Cl₂(C₂₉H₂₅Cl₂FN₄O₉)] (Mw = 962.51): C 36.15, H 3.24, N 8.72; found: C 36.02, H 3.29, N 8.62.

Measurement of Lipophilicity (log P_{o/w}). The shake flask method was used to measure the lipophilicity of the synthesized metal complexes.⁴² Briefly, saturated solutions of PF-I, PF-II, PFB, PFD, and PFL were prepared in water presaturated with *n*-octanol. About half of this stock solution was mixed with an equal volume of octanol presaturated with water, and the mixture was shaken at room temperature for 2 h. Centrifugation was carried out at 12 000g to separate the phases, and the concentration of Pt was measured in initial and final aqueous phase by ICP-MS. The log P_{o/w} was measured using the following equation.

$$\log P_{o/w} = \log([C]_{\text{initial}} - [C]_{\text{final}})/[C]_{\text{final}}$$

Reduction of Pt^{IV} Complexes Analyzed by HPLC. Reduction of Pt^{IV} complexes PF-I and PFL (0.5 mM) was carried out using AA (5 mM) in 0.1 M PBS (Prepared by using 1.37 M NaCl, 27 mM KCl, 100 mM Na₂HPO₄, 18 mM KH₂PO₄ in 1 L of doubly distilled water, and pH is adjusted with NaOH) /MeOH (9/1, V/V, pH 7.4), and the

reduction product was examined at 37 °C by RP-HPLC at different time intervals. Water and methanol was used as a mobile phase for a gradient elution at a flow rate of 1 mL/min. The HPLC elution program was as follows: 5% B (0 min) → 100% B (linear increase in 15 min). The injection volume was 5 μ L.

Stability of Pt^{IV} Complexes Analyzed by HPLC. The stability of PF-I, PF-II, PFD, PFB, and PFL was analyzed in PBS and investigated by HPLC. All complexes were incubated in PBS buffer (pH = 7.4) at 37 °C, and the analysis is performed over a period of 24 h. Reversed-phase HPLC was implemented on a 250 \times 4.5 mm ODS column, and the HPLC profiles were recorded on UV detection at 220 and 266 nm. The percentage of remaining Pt^{IV} compounds were calculated using the ratio of peak area at 266 nm. Water and methanol were used as the mobile phase for a gradient elution at a flow rate of 1 mL/min. The samples were taken for HPLC analysis after filtration by a 0.45 μ m filter.

Cytotoxicity. The cytotoxicity of PF-I, PF-II, PFD, PFB, PFL was assessed using MTT [3-(4,5-dimethylthiazolyl)-2,5-diphenyltetrazolium bromide] assay. Briefly, cells were seeded in a 96-well plate at a density of 2000 cells/well, in 100 μ L of growth medium and were preincubated for 24 h before exposure to the drugs. A stock solution of cDDP was prepared in PBS while PF-I, PF-II, PFD, PFB, and PFL stock solutions were prepared in DMSO. The stock solutions were diluted in a complete medium and then added in aliquots of 100 μ L per well (DMSO concentration <0.5%). After continuing exposure for 72 h, the cells were treated with MTT (20 μ L, 5 mg mL⁻¹ in PBS) for 4 h. The medium was removed, and DMSO (200 μ L) was added to dissolve the purple formazan crystals. The plates were shaken for 10 min and the absorbance of the solution was measured on a Varioskan flash multimode reader (Tokyo, Japan) at 570 nm. Each test was performed in triplicate.

Intracellular Distribution. MDA-MB-231 cells (10⁶) were seeded in 10 cm cell culture dishes using RP-1640 cultural media supplemented with 10% fetal bovine serum. The cells were incubated with PF-I, PF-II, PFD, PFB, PFL or cDDP at a concentration of 10 μ M for 24 h. The cells were washed twice with PBS, collected by trypsin, and resuspended in PBS (1 mL). Mitochondria isolation kit (Beyotime Institute of Biotechnology, China) was used to separate the nuclei, mitochondrion-free cytoplasm, and mitochondria. The isolated fractions were digested with concentrated nitric acid (100 μ L) at 95 °C for 1 h. The solutions were diluted to 1 mL by doubly distilled water. The content of Pt was tested by ICP-MS, and the control value was subtracted.

Annexin V-FITC and PI Staining. MDA-MB-231 cells were seeded in a 6-well cultural plate at a density of 2 \times 10⁵ cells per well. After 20 h of incubation, the medium was replaced with fresh one containing PFL (10 μ M) or cDDP (10 μ M). After an incubation for 48 h, the cells were stained with the Annexin V-FITC assay kit and detected by flow cytometry. Data were analyzed by the Flowjo 7.6.1 software.

Cell Cycle Analysis. MDA-MB-231 cells were seeded in a 6-well plate at a density of 2 \times 10⁵ cells per well. After 20 h of cultivation, the medium was replaced with the fresh one containing PFL (10 μ M) or cDDP (10 μ M). After 48 h, the cells were collected by trypsinization and washed with PBS. The cells were then fixed in ice-cold ethanol (70%) for 6 h, treated with RNase A, and stained with PI in PBS for 15 min. The samples were analyzed by flow cytometry.

Hoechst Staining. MDA-MB-231 cells were treated with cDDP or PFL (15 μ M) for 30 h. After they were fixed with 4% paraformaldehyde for 10 min at room temperature, the cells were washed with PBS twice and stained with Hoechst 33342 (10 μ g/mL, 15 min) in the dark. The samples were washed with PBS again and observed by confocal microscopy. λ_{ex} = 405 nm; λ_{em} = 460 \pm 20 nm.

DNA Platination. MDA-MB-231 cells were seeded in a 10 cm cell cultural dishes at a density of 2 \times 10⁶ cells. After they were incubated at 37 °C for 20 h, the cells were treated with cDDP (15 μ M) or PFL (15 μ M) for 30 h. The attached cells were washed twice with PBS, trypsinized, and washed again with 1 mL of PBS. NucDNA were extracted and purified by commercial spin column quantification kits (AxyPrep Blood gDNA MiniPrep kit). The quantification and purity of DNA were measured by NanoDrop (MD2000, Gene Company

Limited) according to the manufacturer's instructions. The Pt content was quantified by ICP-MS.

Western Blot. The assays were performed according to similar procedures previously reported.⁴³ For TS expression, MDA-MB-231 cells (10⁶) were treated with FT (140 μ M), FTA (140 μ M), PFL (10 μ M), and cDDP (10 μ M) for 48 h. For Bcl-2, Bax, and Cytochrome C expression, MDA-MB-231 cells (10⁶) were treated with cDDP (10 μ M) or PFL (5 and 10 μ M) for 48 h. The cells were collected and lysed by ice-cold RIPA lysis buffer supplemented with protease and phosphatase inhibitor. Protein samples were separated on SDS-PAGE on 12% gel and transferred to a PVDF membrane. The membrane was incubated with primary monoclonal antibodies (Cyto c, Bax, Bcl-2, and α -tubulin) at 4 °C overnight. Subsequently, the membrane was incubated with peroxidase-labeled goat anti-rabbit HRP secondary antibody for 2 h. Western blots were visualized by an enhanced chemiluminescence detection system.

TEM. MDA-MB-231 cells were treated with 10 μ M of PFL at 37 °C for 30 h. The cells were collected and fixed overnight at 4 °C in PBS (pH 7.4) containing 2.5% glutaraldehyde. The cells were then treated with osmium tetroxide, stained with uranyl acetate and lead citrate, and visualized under a transmission electron microscope (JEM 100 CX, JEOL, Tokyo, Japan).

Measurement of MMP. MDA-MB-231 cells were seeded into a 6-well plates at a density of 1 \times 10⁶ cells per well. After an incubation for 20 h, the cells were treated with PFL (10 or 15 μ M) for 30 h. The cells were collected, and the pellets were resuspended in JC-1 staining solutions for 20 min. Fluorescence intensity changes in MDA-MB-231 cells were measured using flow cytometry (FACS Calibur™, Becton Dickinson, NJ). Data were analyzed by FlowJo software (Tree Star, OR).

Mitochondrial Bioenergetics. MDA-MB-231 cells were treated with PFL (5, 10, or 15 μ M) for 30 h at 37 °C. The assay was performed according to the method previously reported.⁴⁴ The key parameters of mitochondrial function were assessed using the XF Cell Mito Stress Test Kit with the Seahorse XFe24 analyzer (Seahorse Bioscience, Billerica) by directly measuring the oxygen consumption rate (OCR) and ECAR according to the manufacturer's instructions.

Intracellular ATP Level. Cellular ATP levels were measured using the Cell Titer-Glo Luminescent Cell Viability assay kit (G7570, Promega, U.S.A.) according to the manufacturer's instructions. MDA-MB-231 cells were seeded in 96-well plates and treated with PFL (10 or 15 μ M) for 30 h. The Cell Titer-Glo reagent was added, and the plate was incubated for 10 min. The luminescence was recorded using a microplate reader (Infinite M200 Pro, Tecan, Switzerland).

Cellular ROS Detection. MDA-MB-231 cells were seeded in 6-well cultural plates at a density of 2 \times 10⁵ cells per well and cultivated for 20 h. The cells were treated with PFL (10 or 15 μ M) for 30 h. The cells were then washed twice with PBS and resuspended in serum-free medium. Cells were stained with H2DCF-DA (10 μ M) at 37 °C for 20 min in the dark. The fluorescence intensity in MDA-MB-231 cells was measured by flow cytometry (FACS Calibur™, Becton Dickinson, U.S.A.). λ_{ex} = 485 nm, λ_{em} = 520 nm.

RNA-seq and Bioinformatics. MDA-MB-231 cells were treated with PFL (10 μ M) for 30 h. Total RNA was purified using RNeasy mini kit (Qiagen, Hilden, Germany). RNA purity was checked using the kaiaoK5500Spectrophotometer (Kaiao, Beijing, China). The integrity and concentration of RNA were assessed using the RNA Nano 6000 Assay Kit (Agilent Technologies, CA). A total amount of 2 μ g RNA per sample was used as input. Sequencing libraries were generated using NEBNext Ultra RNA Library Prep Kit for Illumina (#E7530L, NEB, U.S.A.). RNA concentration of the library was measured using Qubit RNA Assay Kit in Qubit 3.0 to preliminarily quantify and then diluted to 1 ng/ μ L. Insert size was assessed using the Agilent Bioanalyzer 2100 system (Agilent Technologies, CA), and qualified insert size was accurate quantification using StepOnePlus Real-Time PCR System. The libraries were sequenced on an Illumina platform and 150 bp paired-end reads were generated. Sequencing reads were mapped to reference human genome sequence (NCBI 36.1 [hg19] assembly by TopHat (Version 2.0.6). Genes with false discovery rate (FDR) of <0.05 and >200 bp were considered as differentially expressed. Gene

Set Enrichment Analysis (GSEA) was performed following the standard procedure (<http://www.broadinstitute.org/gsea/doc/GSEAUUserGuideFrame.html>) as described by the GSEA user guide.

■ ASSOCIATED CONTENT

SI Supporting Information

The Supporting Information is available free of charge at <https://pubs.acs.org/doi/10.1021/acs.inorgchem.0c01736>.

Supporting experimental methods; characterization of the complexes; stability data; reduction of the complexes by AA; Hoechst staining; ATP assay and RNA-seq data (PDF)

List of genes that are up-regulated or down-regulated (XLSX)

List of transcription factor (TF) genes that are up-regulated or down-regulated (XLSX)

■ AUTHOR INFORMATION

Corresponding Authors

Cai-Ping Tan – MOE Key Laboratory of Bioinorganic and Synthetic Chemistry, School of Chemistry, Sun Yat-sen University, Guangzhou 510275, P. R. China; Email: tancaip@mail.sysu.edu.cn

Zong-Wan Mao – MOE Key Laboratory of Bioinorganic and Synthetic Chemistry, School of Chemistry, Sun Yat-sen University, Guangzhou 510275, P. R. China; orcid.org/0000-0001-7131-1154; Email: cesmzw@mail.sysu.edu.cn

Authors

Nafees Muhammad – MOE Key Laboratory of Bioinorganic and Synthetic Chemistry, School of Chemistry, Sun Yat-sen University, Guangzhou 510275, P. R. China

Uroosa Nawaz – Department of Surgery, P.O.F. Hospital, Wah Cantt 47040, Pakistan

Jie Wang – MOE Key Laboratory of Bioinorganic and Synthetic Chemistry, School of Chemistry, Sun Yat-sen University, Guangzhou 510275, P. R. China

Fang-Xin Wang – MOE Key Laboratory of Bioinorganic and Synthetic Chemistry, School of Chemistry, Sun Yat-sen University, Guangzhou 510275, P. R. China

Sadia Nasreen – Department of Environmental Engineering, University of Engineering & Technology (UET), Taxila 47080, Pakistan

Liang-Nian Ji – MOE Key Laboratory of Bioinorganic and Synthetic Chemistry, School of Chemistry, Sun Yat-sen University, Guangzhou 510275, P. R. China

Complete contact information is available at:

<https://pubs.acs.org/doi/10.1021/acs.inorgchem.0c01736>

Author Contributions

The manuscript was written through contributions of all authors. All authors have given approval to the final version of the manuscript.

Notes

The authors declare no competing financial interest.

■ ACKNOWLEDGMENTS

This study was supported by the National Natural Science Foundation of China (nos. 21778078 and 21837006), the innovative team of Ministry of Education (no. IRT_17R111), the Guangdong Natural Science Foundation

(2015A030306023), and the Fundamental Research Funds for the Central Universities.

■ REFERENCES

- (1) Brewster, A. M.; Chavez-MacGregor, M.; Brown, P. Epidemiology, biology, and treatment of triple-negative breast cancer in women of African ancestry. *Lancet Oncol.* **2014**, *15* (13), e625–e634.
- (2) Turner, N.; Moretti, E.; Siclari, O.; Migliaccio, I.; Santarpia, L.; D'Incalci, M.; Piccolo, S.; Veronesi, A.; Zambelli, A.; Del Sal, G.; Di Leo, A. Targeting triple negative breast cancer: Is p53 the answer? *Cancer Treat. Rev.* **2013**, *39* (5), 541–550.
- (3) Ravera, M.; Gabano, E.; Pelosi, G.; Fregonese, F.; Tinello, S.; Osella, D. A New Entry to Asymmetric Platinum(IV) Complexes via Oxidative Chlorination. *Inorg. Chem.* **2014**, *53* (17), 9326–9335.
- (4) Mayr, J.; Heffeter, P.; Groza, D.; Galvez, L.; Koellensperger, G.; Roller, A.; Alte, B.; Haider, M.; Berger, W.; Kowol, C. R.; Keppler, B. K. An albumin-based tumor-targeted oxaliplatin prodrug with distinctly improved anticancer activity in vivo. *Chem. Sci.* **2017**, *8* (3), 2241–2250.
- (5) Ma, L.; Ma, R.; Wang, Y.; Zhu, X.; Zhang, J.; Chan, H. C.; Chen, X.; Zhang, W.; Chiu, S.-K.; Zhu, G. Chalcoplatin, a dual-targeting and p53 activator-containing anticancer platinum(IV) prodrug with unique mode of action. *Chem. Commun.* **2015**, *51* (29), 6301–6304.
- (6) Muhammad, N.; Guo, Z. Metal-based anticancer chemotherapeutic agents. *Curr. Opin. Chem. Biol.* **2014**, *19*, 144–153.
- (7) Wang, X.; Wang, X.; Jin, S.; Muhammad, N.; Guo, Z. Stimuli-Responsive Therapeutic Metallo-drugs. *Chem. Rev.* **2019**, *119* (2), 1138–1192.
- (8) Bose, R. N.; Moghaddas, S.; Belkacemi, L.; Tripathi, S.; Adams, N. R.; Majmudar, P.; McCall, K.; Dezvareh, H.; Nislow, C. Absence of Activation of DNA Repair Genes and Excellent Efficacy of Phosphaplatins against Human Ovarian Cancers: Implications To Treat Resistant Cancers. *J. Med. Chem.* **2015**, *58* (21), 8387–8401.
- (9) Cheng, Q.; Shi, H.; Wang, H.; Min, Y.; Wang, J.; Liu, Y. The ligation of aspirin to cisplatin demonstrates significant synergistic effects on tumor cells. *Chem. Commun.* **2014**, *50* (56), 7427–7430.
- (10) Ma, J.; Wang, Q.; Huang, Z.; Yang, X.; Nie, Q.; Hao, W.; Wang, P. G.; Wang, X. Glycosylated Platinum(IV) Complexes as Substrates for Glucose Transporters (GLUTs) and Organic Cation Transporters (OCTs) Exhibited Cancer Targeting and Human Serum Albumin Binding Properties for Drug Delivery. *J. Med. Chem.* **2017**, *60* (13), 5736–5748.
- (11) Johnstone, T. C.; Suntharalingam, K.; Lippard, S. J. The Next Generation of Platinum Drugs: Targeted Pt(II) Agents, Nanoparticle Delivery, and Pt(IV) Prodrugs. *Chem. Rev.* **2016**, *116* (5), 3436–86.
- (12) Marrache, S.; Pathak, R. K.; Dhar, S. Detouring of cisplatin to access mitochondrial genome for overcoming resistance. *Proc. Natl. Acad. Sci. U. S. A.* **2014**, *111* (29), 10444.
- (13) Petruzzella, E.; Sirota, R.; Solazzo, I.; Gandin, V.; Gibson, D. Triple action Pt(IV) derivatives of cisplatin: a new class of potent anticancer agents that overcome resistance. *Chem. Sci.* **2018**, *9* (18), 4299–4307.
- (14) Petruzzella, E.; Braude, J. P.; Aldrich-Wright, J. R.; Gandin, V.; Gibson, D. A Quadruple-Action Platinum(IV) Prodrug with Anticancer Activity Against KRAS Mutated Cancer Cell Lines. *Angew. Chem., Int. Ed.* **2017**, *56* (38), 11539–11544.
- (15) Friberg, G.; Schilsky, R. L. Is oral tegafur with leucovorin equivalent to intravenous 5-fluorouracil and leucovorin in colorectal cancer? *Nat. Clin. Pract. Oncol.* **2006**, *3* (5), 240–241.
- (16) Watanabe, T. Evidence produced in Japan: tegafur-based preparations for postoperative chemotherapy in breast cancer. *Breast Canc.* **2013**, *20* (4), 302–309.
- (17) Peng, M.; Ding, Y.; Yu, L.; Deng, Y.; Lai, W.; Hu, Y.; Zhang, H.; Wu, X.; Fan, H.; Ding, H.; Wu, Y.; Tao, G. Tegafur Substitution for 5-Fu in Combination with Actinomycin D to Treat Gestational Trophoblastic Neoplasm. *PLoS One* **2015**, *10* (11), e0143531.
- (18) Lee, S. J.; Choi, Y. L.; Park, Y. H.; Kim, S. T.; Cho, E. Y.; Ahn, J. S.; Im, Y.-H. Thymidylate synthase and thymidine phosphorylase as predictive markers of capecitabine monotherapy in patients with

- anthracycline- and taxane-pretreated metastatic breast cancer. *Cancer Chemother. Pharmacol.* **2011**, *68* (3), 743–751.
- (19) Burdelski, C.; Strauss, C.; Tsourlakis, M. C.; Kluth, M.; Hube-Magg, C.; Mellinger, N.; Lebok, P.; Minner, S.; Koop, C.; Graefen, M.; Heinzer, H.; Wittmer, C.; Krech, T.; Sauter, G.; Wilczak, W.; Simon, R.; Schlomm, T.; Steurer, S. Overexpression of thymidylate synthase (TYMS) is associated with aggressive tumor features and early PSA recurrence in prostate cancer. *Oncotarget* **2015**, *6* (10), 8377–8387.
- (20) Stravopodis, D. J.; Karkoulis, P. K.; Konstantakou, E. G.; Melachroinou, S.; Thanasopoulou, A.; Aravantinos, G.; Margaritis, L. H.; Anastasiadou, E.; Voutsinas, G. E. Thymidylate synthase inhibition induces p53-dependent and p53-independent apoptotic responses in human urinary bladder cancer cells. *J. Cancer Res. Clin. Oncol.* **2011**, *137* (2), 359–374.
- (21) Muhammad, N.; Sadia, N.; Zhu, C.; Luo, C.; Guo, Z.; Wang, X. Biotin-tagged platinum(IV) complexes as targeted cytostatic agents against breast cancer cells. *Chem. Commun.* **2017**, *53* (72), 9971–9974.
- (22) Michelakis, E. D.; Webster, L.; Mackey, J. R. Dichloroacetate (DCA) as a potential metabolic-targeting therapy for cancer. *Br. J. Cancer* **2008**, *99* (7), 989–994.
- (23) Dhar, S.; Lippard, S. J. Mitaplatin, a potent fusion of cisplatin and the orphan drug dichloroacetate. *Proc. Natl. Acad. Sci. U. S. A.* **2009**, *106* (52), 22199.
- (24) Nath, K.; Nelson, D. S.; Heitjan, D. F.; Zhou, R.; Leeper, D. B.; Glickson, J. D. Effects of hyperglycemia on lonidamine-induced acidification and de-energization of human melanoma xenografts and sensitization to melphalan. *NMR Biomed.* **2015**, *28* (3), 395–403.
- (25) Floridi, A.; Gambacurta, A.; Bagnato, A.; Bianchi, C.; Paggi, M. G.; Silvestrini, B.; Caputo, A. Modulation of adriamycin uptake by lonidamine in ehrlich ascites tumor cells. *Exp. Mol. Pathol.* **1988**, *49* (3), 421–431.
- (26) Belzacq, A.-S.; El Hamel, C.; Vieira, H. L. A.; Cohen, I.; Haouzi, D.; Métié, D.; Marchetti, P.; Brenner, C.; Kroemer, G. Adenine nucleotide translocator mediates the mitochondrial membrane permeabilization induced by lonidamine, arsenite and CD437. *Oncogene* **2001**, *20* (52), 7579–7587.
- (27) Moreno-Aspitia, A.; Perez, E. A. Treatment options for breast cancer resistant to anthracycline and taxane. *Mayo Clin. Proc.* **2009**, *84* (6), 533–545.
- (28) Shi, Y.; Liu, S. A.; Kerwood, D. J.; Goodisman, J.; Dabrowiak, J. C. Pt(IV) complexes as prodrugs for cisplatin. *J. Inorg. Biochem.* **2012**, *107* (1), 6–14.
- (29) Wexselblatt, E.; Gibson, D. What do we know about the reduction of Pt(IV) pro-drugs? *J. Inorg. Biochem.* **2012**, *117*, 220–9.
- (30) Basu, U.; Banik, B.; Wen, R.; Pathak, R. K.; Dhar, S. The Platin-X series: activation, targeting, and delivery. *Dalton Trans.* **2016**, *45* (33), 12992–3004.
- (31) Zheng, Y. R.; Suntharalingam, K.; Johnstone, T. C.; Yoo, H.; Lin, W.; Brooks, J. G.; Lippard, S. J. Pt(IV) prodrugs designed to bind non-covalently to human serum albumin for drug delivery. *J. Am. Chem. Soc.* **2014**, *136* (24), 8790–8.
- (32) Ma, L.; Wang, N.; Ma, R.; Li, C.; Xu, Z.; Tse, M.-K.; Zhu, G. Monochalcoplatin: An Actively Transported, Quickly Reducible, and Highly Potent Pt(IV) Anticancer Prodrug. *Angew. Chem., Int. Ed.* **2018**, *57* (29), 9098–9102.
- (33) Zhu, Z.; Wang, Z.; Zhang, C.; Wang, Y.; Zhang, H.; Gan, Z.; Guo, Z.; Wang, X. Mitochondrion-targeted platinum complexes suppressing lung cancer through multiple pathways involving energy metabolism. *Chem. Sci.* **2019**, *10* (10), 3089–3095.
- (34) Wang, K.; Zhu, C.; He, Y.; Zhang, Z.; Zhou, W.; Muhammad, N.; Guo, Y.; Wang, X.; Guo, Z. Restraining Cancer Cells by Dual Metabolic Inhibition with a Mitochondrion-Targeted Platinum(II) Complex. *Angew. Chem., Int. Ed.* **2019**, *58* (14), 4638–4643.
- (35) Fulda, S.; Galluzzi, L.; Kroemer, G. Targeting mitochondria for cancer therapy. *Nat. Rev. Drug Discovery* **2010**, *9* (6), 447–464.
- (36) Nath, K.; Nelson, D. S.; Heitjan, D. F.; Leeper, D. B.; Zhou, R.; Glickson, J. D. Lonidamine induces intracellular tumor acidification and ATP depletion in breast, prostate and ovarian cancer xenografts and potentiates response to doxorubicin. *NMR Biomed.* **2015**, *28* (3), 281–290.
- (37) Green, D. R. Apoptotic Pathways: Ten Minutes to Dead. *Cell* **2005**, *121* (5), 671–674.
- (38) Mymryk, J. S.; Zaniewski, E.; Archer, T. K. Cisplatin inhibits chromatin remodeling, transcription factor binding, and transcription from the mouse mammary tumor virus promoter in vivo. *Proc. Natl. Acad. Sci. U. S. A.* **1995**, *92* (6), 2076–2080.
- (39) Lambert, J. R.; Bilanchone, V. W.; Cumsky, M. G. The ORD1 gene encodes a transcription factor involved in oxygen regulation and is identical to IXR1, a gene that confers cisplatin sensitivity to *Saccharomyces cerevisiae*. *Proc. Natl. Acad. Sci. U. S. A.* **1994**, *91* (15), 7345–7349.
- (40) Zhang, L.; Li, X.; Chao, Y.; He, R.; Liu, J.; Yuan, Y.; Zhao, W.; Han, C.; Song, X. KLF4, a miR-32–5p targeted gene, promotes cisplatin-induced apoptosis by upregulating BIK expression in prostate cancer. *Cell Commun. Signaling* **2018**, *16* (1), 53.
- (41) Nagatani, G.; Nomoto, M.; Takano, H.; Ise, T.; Kato, K.; Imamura, T.; Izumi, H.; Makishima, K.; Kohno, K. Transcriptional Activation of the Human HMG1 Gene in Cisplatin-resistant Human Cancer Cells. *Cancer Res.* **2001**, *61* (4), 1592.
- (42) Ang, W. H.; Khalaila, I.; Allardyce, C. S.; Juillerat-Jeanneret, L.; Dyson, P. J. Rational design of platinum(IV) compounds to overcome glutathione-S-transferase mediated drug resistance. *J. Am. Chem. Soc.* **2005**, *127* (5), 1382–3.
- (43) Liu, Z.; Wang, M.; Wang, H.; Fang, L.; Gou, S. Platinum-Based Modification of Styrylbenzylsulfones as Multifunctional Antitumor Agents: Targeting the RAS/RAF Pathway, Enhancing Antitumor Activity, and Overcoming Multidrug Resistance. *J. Med. Chem.* **2020**, *63* (1), 186–204.
- (44) Yang, J.; Cao, Q.; Zhang, H.; Hao, L.; Zhou, D.; Gan, Z.; Li, Z.; Tong, Y.-X.; Ji, L.-N.; Mao, Z.-W. Targeted reversal and phosphorescence lifetime imaging of cancer cell metabolism via a theranostic rhenium(I)-DCA conjugate. *Biomaterials* **2018**, *176*, 94–105.